

Solid-liquid phase equilibria of the Gaussian core model fluid

Peter Mausbach,¹ Alauddin Ahmed,² and Richard J. Sadus^{2,a)}¹*Cologne University of Applied Sciences, 50679 Cologne, Germany*²*Centre for Molecular Simulation, Swinburne University of Technology, P.O. Box 218, Hawthorn, Victoria 3122, Australia*

(Received 31 August 2009; accepted 6 October 2009; published online 12 November 2009)

The solid-liquid phase equilibria of the Gaussian core model are determined using the GWTS [J. Ge, G.-W. Wu, B. D. Todd, and R. J. Sadus, *J. Chem. Phys.* **119**, 11017 (2003)] algorithm, which combines equilibrium and nonequilibrium molecular dynamics simulations. This is the first reported use of the GWTS algorithm for a fluid system displaying a reentrant melting scenario. Using the GWTS algorithm, the phase envelope of the Gaussian core model can be calculated more precisely than previously possible. The results for the low-density and the high-density (reentrant melting) sides of the solid state are in good agreement with those obtained by Monte Carlo simulations in conjunction with calculations of the solid free energies. The common point on the Gaussian core envelope, where equal-density solid and liquid phases are in coexistence, could be determined with high precision. © 2009 American Institute of Physics. [doi:10.1063/1.3256004]

I. INTRODUCTION

Determining the solid-liquid phase transition via molecular simulation remains a considerable challenge. The most commonly used options are thermodynamic integration methods¹ based on the evaluation of free energies; Gibbs ensemble simulation,^{2,3} which requires particle interchanges between two dense phases, and Gibbs–Duhem integration (GDI).⁴ In particular, GDI is a very useful method for studying solid-liquid phase transitions because it avoids the issue of particle interchanges between phases. However, GDI requires *a priori* knowledge of a pair of coexistence points to start the algorithm, and the accuracy of the starting conditions is of great importance for its success. The solid-liquid transition can be calculated from direct simulation of an inhomogeneous system formed from liquid and solid phases separated by an interface. However, as noted recently elsewhere,⁵ very long simulation times are sometimes required to obtain reliable results, which also places a computational restriction on the number of particles that can be feasibly simulated.

An alternative to these conventional approaches was introduced by Ge *et al.*⁶ using a combination of equilibrium molecular dynamics (EMD) and nonequilibrium molecular dynamics (NEMD) simulation methods.³ We will use the designation “GWTS” (after the first letter of the surnames of the authors) to refer to this algorithm. The GWTS algorithm allows for an efficient localization of the freezing point (fp) by applying small strain rates to the system. A change in the strain-rate dependent pressure as a function of density indicates the occurrence of the fp. The coexisting melting point (mp) can be easily obtained from an isobaric connection of the fp to the solid branch. The fast and accurate determination of the solid-liquid transition at equilibrium for a one-component Lennard-Jones system has been demonstrated.⁶

The GWTS algorithm provides a powerful alternative to other simulation techniques^{1–4} because it is both self-starting and it does not require particle interchanges between the dense liquid and solid phases.

The aim of this study is to apply the GWTS algorithm⁶ to accurately determine solid-liquid equilibria of the Gaussian core model (GCM) fluid. The GCM system displays a complex thermodynamic melting scenario, the so-called reentrant melting, where the solid remelts into a stable high-density liquid. For temperatures lower than a maximum melting temperature T_{\max} , a liquid-solid-liquid sequence of phases can be observed when increasing the density. This behavior has been observed in the phase diagram of elements such as barium, caesium, carbon, and phosphorus.⁷ Furthermore, the GCM is a bounded, solely repulsive interaction potential, which has been used to describe properties of soft materials.⁸ For example, the GCM provides a reliable qualitative description of the thermal behavior of interpenetrable globular polymers.

In the past, different approaches have been applied to observe the topology of the GCM phase diagram.^{9–11} Currently, the most accurate simulation results were reported by Prestipino *et al.*¹² using Monte Carlo simulations in conjunction with calculations of the solid free energies. Compared with the results reported by Prestipino *et al.*,¹² the one-phase entropy criterion¹¹ underestimates T_{\max} by approximately 30%. In contrast, the approach used by Lang *et al.*¹⁰ yields a value of T_{\max} that is approximately 10% higher than reported by Prestipino *et al.*¹² Furthermore, the calculations reported by Prestipino *et al.*¹² lead to a partially modified phase diagram for the face centered cubic-body centered cubic (fcc-bcc) solid transition compared with previous calculations.^{9,10} To the best of our knowledge, the successful use of direct coexistence methods for GCM-like fluids has not been reported. In view of these considerations, the GCM fluid provides a severe test for the GWTS algorithm. It should be

^{a)}Electronic mail: rsadus@swin.edu.au.

noted that because the GWTS algorithm uses liquid state simulation methods, it can not be used to determine solid-solid transitions.

II. SIMULATION METHOD

A. Brief overview of the GWTS algorithm

Conducting standard EMD simulations close to the solid-liquid phase boundary allows an extension of the stable liquid and the stable solid line into the metastable two-phase solid-liquid region of the system. This effect, known as a van der Waals loop, makes it difficult to determine the exact location of the phase transition. However, when the system enters the two-phase liquid-solid region from the liquid side the equilibrium pressure drops considerably. In principle, one could use the drop in the equilibrium pressure to determine the freezing transition of the system. However, such an approach would not work for systems like the GCM, which do not exhibit any significant difference in pressure. The GWTS algorithm⁶ utilizes the fact that a small strain rate applied to a system disturbs its two-phase state. By conducting additional NEMD simulations at low strain rates and analyzing the strain-rate dependent pressure, it is relatively easy to determine whether the system is in the single liquid phase, the two-phase state, or the solid phase. The entry into the two-phase liquid-solid region is clearly identified by a sudden change in the pressure at zero strain rate, whereas the pressure at $\dot{\gamma} > 0$ remains almost linear with increasing $\dot{\gamma}$. As discussed by Ge *et al.*⁶ this is an entirely empirical observation. However, the large drop in pressure can be attributed to the sensitivity of the NEMD symmetric and asymmetric pressure tensors to changes in the structure of the fluid at the freezing transition. Once the fp has been determined in this way, it is straightforward to determine the mp by extending an isobaric tie line from the fp to the solid branch curve. Starting in the liquid phase, increasing the density at constant temperature in incremental amounts of $\Delta\rho$ (the situation when reentrant melting occurs will be discussed later) determines the equilibrium coexistence of the solid-liquid phase transition with an accuracy of $\Delta\rho$. In contrast to direct coexistence methods,⁵ the absence of a physical interface means that computational difficulties³ at the interfacial region are avoided.

B. Simulation details

In this study the interaction between particles is described by a potential with a Gaussian core (GC) shape, i.e.,

$$u(r) = \varepsilon \exp\left[-\left(\frac{r}{\sigma}\right)^2\right], \quad (1)$$

where σ is the length scale and ε is the energy scale of the model. All the results are given in a system of reduced GC units that is natural for the model.^{13–15} In particular, we report density ($\rho^* = \rho\sigma^3$), temperature ($T^* = kT/\varepsilon$), pressure ($p^* = p\sigma^3/\varepsilon$), strain-rate ($\dot{\gamma}^* = \dot{\gamma}\sqrt{m\sigma^2/\varepsilon}$), and time ($\tau^* = \tau\sqrt{\varepsilon/m\sigma^2}$) in terms of these reduced quantities. The asterisk superscript will be omitted in the rest of this study.

Homogeneous NEMD simulations were conducted by

TABLE I. System size dependency of the freezing density of the GCM fluid at $T=0.006$ obtained using the GWTS algorithm.

N	ρ
256	0.1309
864	0.1291
2048	0.1299
4000	0.1299
6912	0.1304
10 976	0.1297

applying the standard *slod* equations¹⁶ of motion and a Gaussian thermostat¹⁷ was used to constrain the kinetic temperature. The equations of motion were integrated with a five-value Gear predictor-corrector scheme^{3,18} with a time step of $\tau=0.005$ and a cutoff radius for the potential of 3.2σ . We used three different strain rates at $\dot{\gamma}=0.0$ (EMD simulation), $\dot{\gamma}=0.001$, and $\dot{\gamma}=0.002$ (NEMD simulations). For each state point ($\rho, T, \dot{\gamma}$) simulation trajectories were made for a length of $8 \times 10^5 \tau$. Periods of $3 \times 10^5 \tau$ of each trajectory were used either to equilibrate zero-shearing field EMD or to achieve nonequilibrium steady state after the shearing field was switched on. The remaining time periods were used to accumulate the average values of thermodynamic variables. We used 2048 GC particles for all simulations reported in this work. Near the solid-liquid transition we used very small density increments $\Delta\rho=10^{-4}$ in order to sample the extremely small two-phase liquid-solid region of the GCM with high accuracy.

C. System size analysis

Simulation of phase transitions might be sensitive to the system size of a fluid. Therefore, we performed separate simulation runs to analyze the dependency of the simulation results on the particle number. In particular, we calculated the fp on the low-density side of the solid region of the GCM for a single temperature at $T=0.006$. We analyzed the occurrence of the fp for system sizes of $N=256, 864, 2048, 4000, 6912$, and $10\,976$ particles (Table I). The average freezing density calculated from Table I is $0.129\,983 \pm 0.000\,492$ within a 95% confidence interval. The freezing density obtained for $N=2048$ fits fairly well within the average density, which suggests that this number of particles is a good choice for the purpose of our study.

III. RESULTS AND DISCUSSION

A. Low-density side of the solid region

On the low-density side of the solid state the GCM fluid behaves as a “normal” liquid.¹³ In Fig. 1 we show a typical result of our simulation in this density region for a temperature of $T=0.006$. The strain-rate dependent pressure is shown in Fig. 1(a) for a density range of $\rho=0.1296–0.1305$ in steps of $\Delta\rho=10^{-4}$. Up to a density of 0.1299 the system is still in the liquid state because the pressure is nearly constant for all three strain rates. Increasing the density to 0.13 results in a sudden drop in the pressure at zero strain rate. For densities $\rho \geq 0.13$ the equilibrium pressures are even lower than those

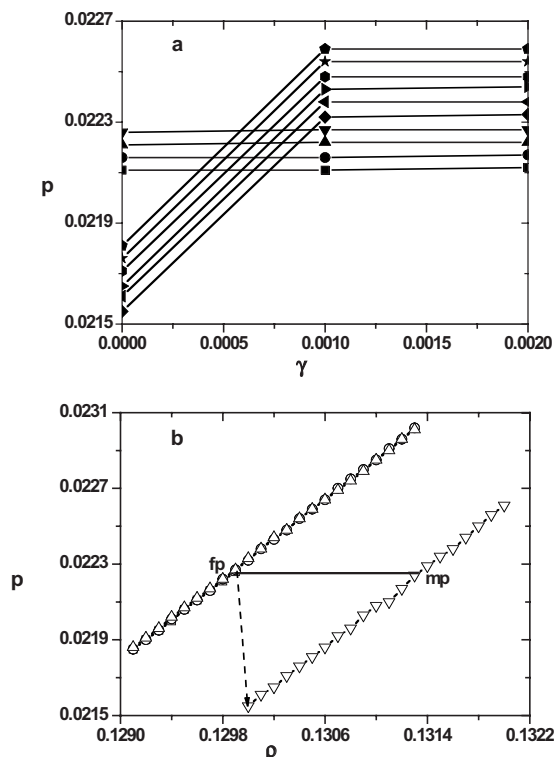


FIG. 1. Low-density side of the GCM solid state at $T=0.006$. (a) Pressure as a function of strain rate at different constant densities. Shown are results for densities of 0.1296 (■), 0.1297 (●), 0.1298 (▲), 0.1299 (▼), 0.1300 (◆), 0.1301 (◄), 0.1302 (►), 0.1303 (●), 0.1304 (★), and 0.1305 (●). Entry into the two-phase solid-liquid region is clearly seen by the sudden drop in pressure at zero strain rate. (b) Pressure as a function of density for different strain rates $\dot{\gamma}=0.0$ (□), $\dot{\gamma}=0.001$ (○), $\dot{\gamma}=0.002$ (△), all in the stable liquid state and its metastable extension, and $\dot{\gamma}=0.0$ (▽) in the stable solid state and its metastable extension. The symbols fp and mp refer to the freezing point and the melting point, respectively. A dashed arrow marks the drop in the equilibrium pressure.

for $\rho \leq 0.1296$. This indicates the entry into the two-phase solid-liquid region, i.e., the fp. To determine the mp we plot the results in the pressure-density plane in Fig. 1(b). The curves for strain rates at $\dot{\gamma}=0.0$, 0.001, and 0.002 nearly lie on top of each other in the liquid branch. A dashed arrow marks the drop in the equilibrium pressure starting at fp. The pressures for strain rates at $\dot{\gamma}=0.001$ and 0.002 extend from the stable liquid branch into the two-phase solid-liquid region. Drawing an isobaric line from fp to the solid branch identifies mp. The construction at $T=0.006$ yields densities of $\rho_f=0.1299$ and $\rho_m=0.13134$. On the low-density side we calculated transitions at $T=0.002$, 0.004, 0.006, 0.008, and 0.0089 and the results are summarized in Table II.

B. High-density side of the solid region

On the high-density side of the solid state, where overlapping of particles becomes important, the GCM fluid displays reentrant melting into the stable liquid state. Contrary to the normal case, the liquid coexisting with the solid has a higher density than the solid. In this region we have to reverse our method in the sense that we have to start in the liquid phase at higher densities and decrease the density in order to enter the two-phase solid-liquid region. In Fig. 2 we show the results for the high-density (reentrant melting) re-

TABLE II. Freezing and melting densities for the low-density and high-density sides of the solid state of the GCM fluid obtained using the GWTS algorithm.

T	Low-density side		High-density side	
	ρ_f	ρ_m	ρ_m	ρ_f
0.002	0.0761	0.078 17	0.720 97	0.7215
0.004	0.1017	0.103 57	0.541 99	0.5429
0.006	0.1299	0.131 34	0.432 79	0.4338
0.008	0.1687	0.169 60	0.332 88	0.3337
0.0089	0.2124	0.212 70
0.009	0.256 26	0.2565

gion for a temperature of $T=0.004$. The strain-rate dependent pressure for densities ranging from $\rho=0.5433$ to 0.5424 is shown in Fig. 2(a). Down to a density of 0.5429 the system is still in the liquid phase. The interesting fact in this region is that opposite to the low-density side, the equilibrium pressure jumps up to higher values for densities $\rho \leq 0.5428$. At a density of $\rho_f=0.5429$ we find the fp. The pressure-density projection of the results is shown in Fig. 2(b). Again, the curves for strain rates at $\dot{\gamma}=0.0$, 0.001, and 0.002 nearly lie on top of each other in the liquid branch. A dashed arrow marks the jump of the equilibrium pressure. An analogous

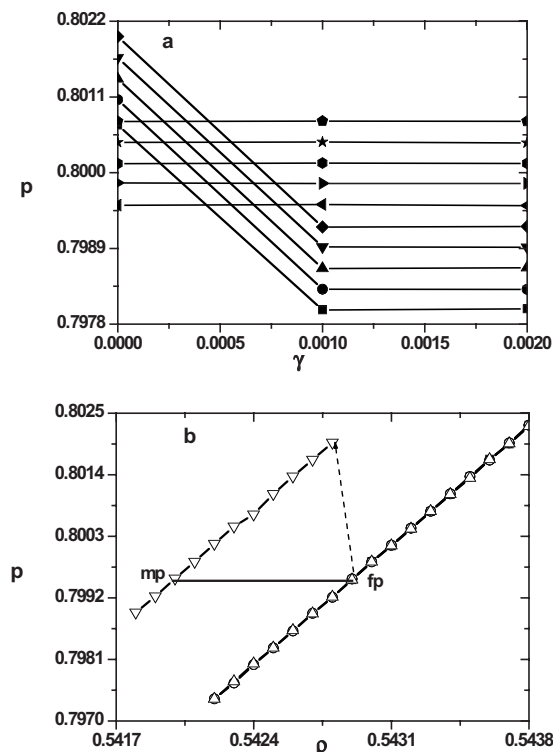


FIG. 2. High-density side of the GCM solid state at $T=0.004$. (a) Pressure as a function of strain rate at different densities. Shown are results for the densities of 0.5424 (■), 0.5425 (●), 0.5426 (▲), 0.5427 (▼), 0.5428 (◆), 0.5429 (◄), 0.5430 (►), 0.5431 (●), 0.5432 (★), and 0.5433 (●). Entry into the two-phase solid-liquid region is clearly seen by the sudden jump in pressure at zero strain rate. (b) Pressure as a function of density for different strain rates $\dot{\gamma}=0.0$ (□), $\dot{\gamma}=0.001$ (○), $\dot{\gamma}=0.002$ (△), all in the stable liquid state and its metastable extension, and $\dot{\gamma}=0.0$ (▽) in the stable solid state and its metastable extension. The symbols fp and mp refer to the freezing point and the melting point, respectively. A dashed arrow marks the jump in the equilibrium pressure.

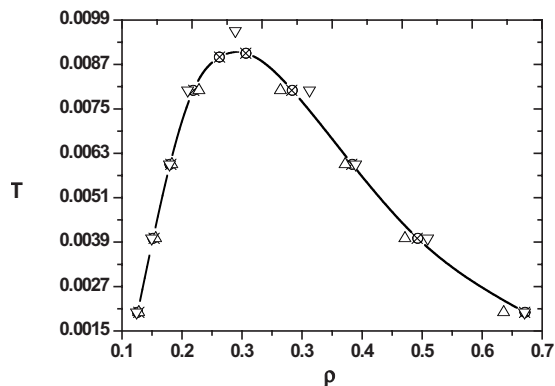


FIG. 3. Phase diagram of the GCM fluid showing the freezing (○) and melting lines (×) obtained in this work. The fps (△) reported by Prestipino *et al.* (Ref. 12) and freezing thresholds (▽) predicted by the Hansen-Verlet rule (Ref. 19) are also illustrated.

construction of mp yields a melting density of $\rho_m = 0.54199$. On the high-density side we calculated transitions at $T=0.002$, 0.004, 0.006, 0.008, and 0.009 and the results are summarized in Table II.

C. The GCM phase diagram

In Fig. 3 we show our results for the solid-liquid phase coexistence at equilibrium and compare them with the currently most accurate simulation results of Prestipino *et al.*¹² In addition, we also show freezing thresholds¹⁹ predicted by the Hansen-Verlet rule based on the height of the first peak of the structure factor at freezing. Lang *et al.*¹⁰ established that the phase boundaries of the GCM are well reproduced by the Hansen-Verlet criterion. In general, the coexistence lines are double lines, but they cannot be resolved on the scale of the figure because the solid-liquid density gap is too small. On the low-density side our results are in very good agreement with those of Prestipino *et al.*¹² The solid region in our simulation is broader at higher temperatures ($T=0.008$). This tendency continues on the high-density side where the melting and the freezing lines are shifted slightly to higher densities, compared with those obtained by Prestipino *et al.*¹² At almost all temperatures studied, the liquid

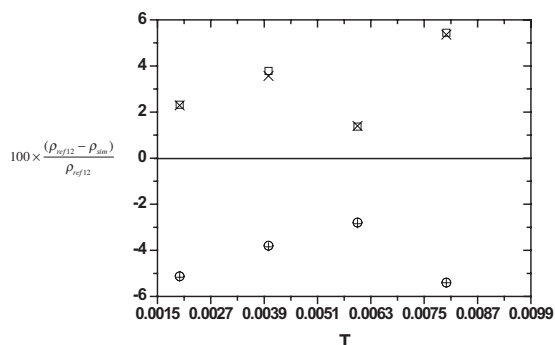


FIG. 4. Comparison of the relative percentage difference in freezing (□) and melting (×) densities on the low-density side and freezing (○) and melting (+) densities on the high-density side at different temperatures obtained in this work with data reported in Ref. 12.

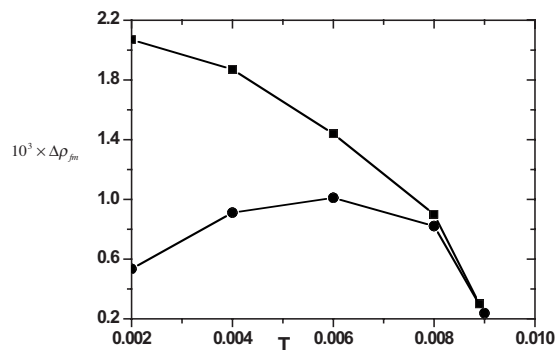


FIG. 5. The solid-liquid density gap $\Delta\rho_{fm} = |\rho_f - \rho_m|$ on the low-density (■) and high-density (●) sides of the GCM phase diagram as a function of temperature.

phase is transformed into a bcc solid. The only exception is the low-density side at $T=0.002$ where the liquid phase is transformed into a fcc solid.

Figure 4 provides a quantitative comparison of our coexistence densities to those obtained from Prestipino *et al.*¹² The comparison indicates that at any temperature, the discrepancies between the two calculation methods are typically less than 5%. Our results are in between the values reported by Prestipino *et al.*¹² and the predictions of the Hansen-Verlet freezing rule.¹⁹

In Fig. 5 we show the solid-liquid density gap $\Delta\rho_{fm} = |\rho_f - \rho_m|$ on the low-density and the high-density sides depending on temperature. The density gap is larger on the low-density side. For both density sides the density difference decreases when increasing the temperature for $T \geq 0.006$. Extrapolating the density gaps to temperatures higher than $T=0.009$ suggests that the two-phase solid-liquid region disappears completely for both density sides at a common point, as predicted by Stillinger,²⁰ with a maximum freezing/melting temperature T_{max} . We located this maximum value at $T_{max} = 0.00903$ for $\rho_{max} = 0.24265$. This compares with maximum values $T_{max} = 0.00874$ for $\rho_{max} = 0.239$ obtained by Prestipino *et al.*¹²

IV. CONCLUSIONS

Determining solid-liquid phase transitions of the GCM fluid is a severe test for the GWTS algorithm because the GC model has a very small range of densities in which phase separation can occur and it has a complex reentrant melting scenario. Using the GWTS algorithm, the phase envelope of the GC potential can be calculated very precisely. Our results are consistent with that of other work.¹² On the high-density side the solid-liquid coexisting line is slightly shifted to higher densities compared with the results of Prestipino *et al.*¹² The common point, predicted by Stillinger,²⁰ where the crystal and its melt have the same density, could be determined with high precision. The common point on the GC envelope has not been resolved so far and a detailed analysis will be of considerable interest. We believe that using the GWTS algorithm can also contribute to the understanding of other unusual phase diagram topologies.

ACKNOWLEDGMENTS

Financial support from the Deutsche Forschungsgemeinschaft (DFG) is gratefully acknowledged. We thank Santi Prestipino for providing numerical values of the simulation data reported graphically in Ref. 12, which were used for comparison in Figs. 3 and 4. One of us (A.A.) thanks Swinburne University of Technology for a postgraduate scholarship.

¹J. P. Hansen and L. Verlet, *Phys. Rev.* **184**, 151 (1969).

²A. Z. Panagiotopoulos, *Mol. Phys.* **61**, 813 (1987).

³R. J. Sadus, *Molecular Simulation of Fluids: Theory, Algorithms, and Object-Oriented* (Elsevier, Amsterdam, 1999).

⁴D. A. Kofke, *J. Chem. Phys.* **98**, 4149 (1993); R. Agrawal and D. A. Kofke, *Mol. Phys.* **85**, 43 (1995).

⁵R. García Fernández, J. L. F. Abascal, and C. Vega, *J. Chem. Phys.* **124**, 144506 (2006).

⁶J. Ge, G.-W. Wu, B. D. Todd, and R. J. Sadus, *J. Chem. Phys.* **119**, 11017 (2003).

⁷D. A. Young, *Phase Diagrams of the Elements* (University of California Press, Berkeley, 1991).

⁸C. N. Likos, *Phys. Rep.* **348**, 267 (2001).

⁹F. H. Stillinger and D. K. Stillinger, *Physica A* **244**, 358 (1997).

¹⁰A. Lang, C. N. Likos, M. Watzlawek, and H. Löwen, *J. Phys.: Condens. Matter* **12**, 5087 (2000).

¹¹P. V. Giaquinta and F. Saija, *ChemPhysChem* **6**, 1768 (2005).

¹²S. Prestipino, F. Saija, and P. V. Giaquinta, *Phys. Rev. E* **71**, 050102(R) (2005).

¹³P. Mausbach and H.-O. May, *Fluid Phase Equilib.* **249**, 17 (2006).

¹⁴P. Mausbach and H.-O. May, *Z. Phys. Chem.* **223**, 1035 (2009).

¹⁵A. Ahmed, P. Mausbach, and R. J. Sadus (to be published).

¹⁶D. J. Evans and G. P. Morriss, *Statistical Mechanics of Nonequilibrium Liquids*, 2nd ed. (Academic, New York, 2008).

¹⁷D. J. Evans, W. G. Hoover, B. H. Failor, B. Moran, and A. J. C. Ladd, *Phys. Rev. A* **28**, 1016 (1983).

¹⁸C. W. Gear, *Numerical Initial Value Problems in Ordinary Differential Equations* (Prentice-Hall, Englewood Cliffs, NJ, 1971).

¹⁹F. Saija, S. Prestipino, and P. V. Giaquinta, *J. Chem. Phys.* **124**, 244504 (2006).

²⁰F. H. Stillinger, *J. Chem. Phys.* **65**, 3968 (1976).